ISSN 1330-3651 (Print), ISSN 1848-6339 (Online) https://doi.org/10.17559/TV-20220809151506
Original scientific paper

Determining Singularity-Free Inner Workspace through Offline Conversion of Assembly Modes for a 3-RRR PPM

Yin GAO*, Ke CHEN, Hong GAO, Hongmei ZHENG, Lulu WU, Ping XIAO

Abstract: The existing singularity avoidance methods have deficiencies, such as the conditionality of the online conversion of the assembly modes (AMs) and the kinematically redundant manipulator with the predicament of the prototype design and added complexity of the mechanism. To address these issues, a method to determine a singularity-free inner workspace through offline conversion of the AMs of the 3-RRR planar parallel manipulator (PPM) is presented. Based on the geometric relations among rods of the manipulator during the occurrence of singularity, and the singular points at or near the boundary of the workspace are permitted, the AMs and ranges of the orientation angle of the moving platform corresponding to the inner singularity-free workspace are determined through a three-dimensional search method. The simulation and experimental comparisons indicate that singular-free paths related to the constant or variable orientation angle of the moving platform can be planned on the singularity-free inner workspace.

Keywords: 3-RRR PPM; first or second type of singularity; geometric relations among rods of the manipulator; offline conversion of AMs; inner singularity-free workspace

1 INTRODUCTION

General parallel mechanisms, such as the Stewart platform and delta robot, have been widely applied [1-3]. The 3-RRR planar parallel manipulator (PPM) is a type of special parallel mechanism that has received much attention from researchers and has been studied under varying conditions. Micro-motion stages with basic structural schemes based on the 3-RRR PPM are widely applied in position sampling in scanning electron microscopy and haptic sensors [4-6].

Investigations of the 3-RRR PPM mainly involve modelling kinematics and assembly modes (AMs) [6-8], workspaces [9-15], singularity analysis [7, 8, 16-22], and the dynamics and optimisation of actuator power consumption [23, 24].

There are several important research findings on the workspace and singularities that are closely linked with workspaces. In the studies conducted on the method and results of workspace determination for the 3-RRR PPM, three methods have been proposed: the kinematic chain dismantling approach based on Euclidean geometry [9-11], the discretising method based on computer-aided technology [12], and the method of combining analysis with a numerical solution [13-15] to deal with the relevant issues.

The ultimate goal of singularity research is to provide a theoretical basis and implementation method for avoiding singularities [7, 8, 15-18]. The first, second and third type of singularity were researched for 3-RRR manipulator [16], and the phenomena of the gain singularities were discussed and further analyzed through the constraint equations [17]. It is noteworthy that a control scheme to avoid singularity had been proposed through the modification dynamically for the behaviour of the manipulator [18]. At the same time, the kinematically redundant manipulator [19-22], online conversion for AMs [7], and small-angle perturbation for the moving platform (SAPMP) [8] are the primary means through which the singularity of the 3-RRR PPM is avoided. It is worth noting that the conversion of AMs or SAPMP [7, 8] does not change the non-redundancy of the 3-RRRPPM. For convenience of expression, the conversion of AMs or SAPMP is called the non-redundant singularity avoidance method (NRSAM), which adopts the non-redundant 3-RRRPPM with only seven rods and nine kinematic pairs.

The singularity avoidance problem of the mechanism can be solved without changing the degree of freedom of the mechanism by using redundant kinematic chains [19, 20]; however, at least one redundant branch chain is added. In such a case, the number of inverse solutions is increased to 16. Furthermore, when two redundant branch chains are added, the number of inverse solutions is increased to 32; accordingly, the number of AMs (or working modes) is also increased to 32, which evidently increases the complexity of practical applications. Simultaneously, avoiding interference between the rods during prototype design is a new challenge. Several solutions have been proposed to avoid singular trajectories in the mechanism. For example, three feasible kinematic redundancy configurations were presented, and an effective algorithm pertaining to the kinematic redundancy of the mechanisms was realised [21] by expanding upon on the research presented in previous studies [22]. The artificial potential function was chosen in close proximity to the singular points to modify the dynamic behaviour of the moving platform; therefore, the singular points of the mechanism were avoided without changing the planned path [22]. Hence, the scheme of kinematic redundancy [19-22] inevitably increases the number of rods and sliding or rotating pairs, resulting in a predicament during the prototype design; accordingly, the complexity of the mechanism and accumulative error are increased.

In addition, a path-planning method to use online conversion among different AMs of the 3-RRR PPM was also presented by several researchers [7]. Although the online conversion for AMs is an NRSAM, this method is feasible only when different AMs can be transformed during the mechanism motion. In other words, if there is no overlapping area in the motion range of the active rods related to different AMs, this method cannot be implemented [8].

The theory of the singularity for the 3-RRR PPM has been researched by literatures [15], [16] and [17]. On this basis, the geometric relations among rods of the mechanism are fully taken into account when the

determinants of the discriminant matrix for the first and second type of singularity of the 3-RRR PPM are equal to zero [7, 8, 15-17]; by further investigating the sufficient condition of the first type of singularity for the 3-RRR PPM [15-17], it is found that the first type of singularity of the 3-RRR PPM occurs if the condition that the active and passive rods in the same branch chain are straightened or overlapped on the same straight line is true. Under such a circumstance, the centroid of the moving platform is located at the boundary of the workspace. Conversely, by investigating the necessary and sufficient condition of the second type of singularity for the 3-RRR PPM [15-17], it can be easily surmised that the online conversion of AMs [7] or SAPMP [8] can avoid the second type of singularity because the relative geometric positions among the three passive rods are changed through the conversion of AMs or SAPMP when the singularity of the 3-RRR PPM occurs. For these reasons, considering the conditionality of the online conversion of AMs, a method to determine the singularity-free inner workspace through offline conversion of AMs of the 3-RRR PPM is presented as a further supplement to the NRSAM.

The implementation of the method only adopts the non-redundant 3-RRRPPM with seven rods and nine kinematic pairs, and no extra rods and kinematic pairs are added; therefore, the method is easier to apply in engineering. Meanwhile, permitting the singularity of some boundary points, aiming at eight different AMs, the corresponding AMs and orientation range of the moving platform are determined by a three-dimensional search method when there is no second type of singularity in the inner workspace, except for points at or near the boundary. The proposed method is particularly suitable for handling cases in which there is no overlapping area in the motion range of the active rods related to the different AMs. In the determined singularity-free inner workspace, the singularity-free motion along the planned path can be realised without the online conversion of AMs through only one assembly and disassembly according to the corresponding AM.

Considering the 3-RRR PPM as the research object, this paper is structured as follows. The basic theories related to the 3-RRR PPM, such as inverse displacement, AMs, singularity, workspace, the sufficient condition of the first type of singularity and the probable distribution of the first type of singularity in the workspace, and the necessary and sufficient condition of the second type of singularity for the 3-RRR PPM are discussed in Section 2. The method to avoid the second type of singularity based on offline conversion of AMs for the 3-RRR PPM is discussed geometrically, implemented by a computer software, and verified by an experiment in an example in Section 3. Finally, conclusions are presented in Section 4.

2 INVERSE DISPLACEMENT, AMs, SINGULARITY, AND WORKSPACE

2.1 Inverse Displacement for the 3-RRR PPM

The 3-RRR PPM is composed of a framework, three active rods, three passive rods, and a moving platform. As shown in Fig. 1, the framework is the triangle $A_1A_2A_3$. Active rods A_1B_1, A_2B_2, and A_3B_3 are linked to the framework at points A_1, A_2, and A_3 by revolute hinges. One side of the passive rods B_1C_1, B_2C_2, and B_3C_3 is linked to the active rods at points B_1, B_2, and B_3 by revolute hinges; the other side is linked to the moving platform, which is the triangle $C_1C_2C_3$, at points C_1, C_2, and C_3, by revolute hinges [7, 8].

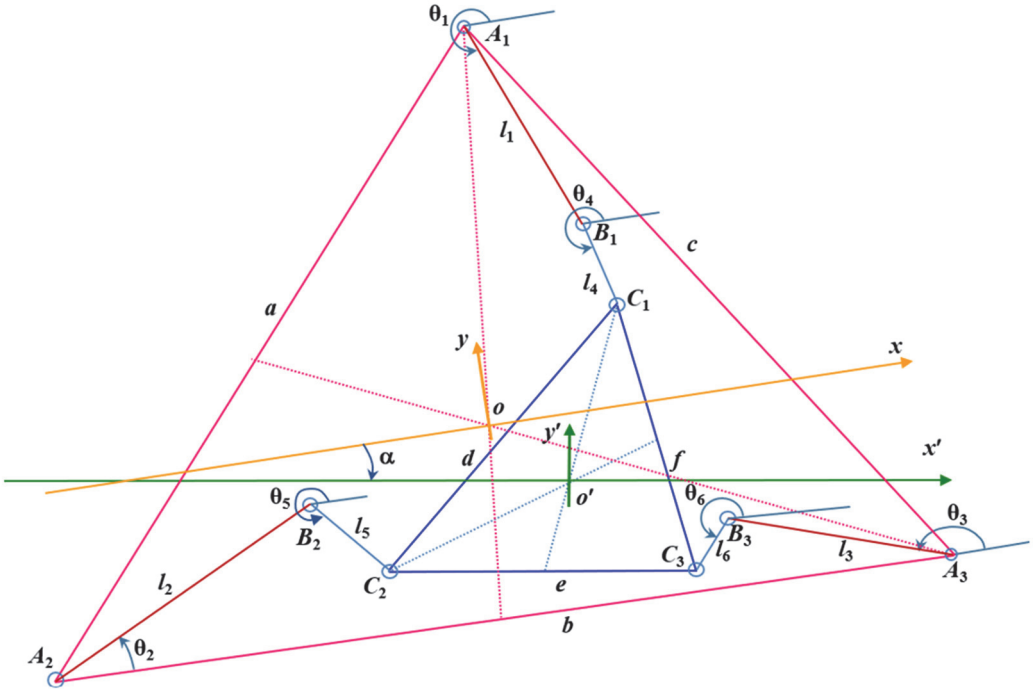

Figure 1 Kinematic sketch of the 3-RRR PPM and coordinate systems

A global coordinate system oxy is established, where the origin o is the circumcentre of the triangle $A_1A_2A_3$, and the x-coordinate axis is through the point o and parallel to the line A_2A_3. The local coordinate system $o'x'y'$ is fixed to the moving platform $C_1C_2C_3$, where the origin o' is the circumcentre of the triangle $C_1C_2C_3$, and the x'-axis is through the point o' and parallel to the line C_2C_3. The

rotation angle α of the x'-axis relative to the x-axis is defined as the orientation angle of the moving platform (the counter clockwise direction is positive).

For convenience, the meaning and symbols of the primary parameters of the 3-RRR PPM are listed in Tab. 1.

Table 1 Primary parameters for the 3-RRR PPM (i = 1, 2, 3)

Meaning	Symbol	Meaning	Symbol
Lengths of sides of the triangle $A_1A_2A_3$	a, b, c	Lengths of sides of the triangle $C_1C_2C_3$	d, e, f
Lengths of the active rods A_iB_i	l_i	Rotation angle of the active rod A_iB_i	θ_i
Length of the passive rod B_iC_i	$l_{(i+3)}$	Rotation angle of the passive rod B_iC_i	θ_{i+3}
Global coordinate of the central point o' of the moving platform	(x, y)	Orientation angle of the moving platform	α
Global coordinates of the points A_i	(x_{Ai}, y_{Ai})	Global coordinates of the points B_i	(x_{Bi}, y_{Bi})
Global coordinates of the points C_i	(x_{Ci}, y_{Ci})	Local coordinates of the points C_i	(x_{Ci}', y_{Ci}')
Discriminant matrix of the first type of singularity	$\boldsymbol{\Phi}_z$	Discriminant matrix of the second type of singularity	$\boldsymbol{\Phi}_y$
Augmented matrix from the equations of the straight line B_iC_i	$\boldsymbol{\Phi}_C$		

When the inverse solution is obtained, the known conditions are as follows: (1) the global coordinate (x, y) of the central point o' of the moving platform; (2) the orientation angle α of the moving platform; (3) all dimensional parameters l_i and l_{i+3} of the 3-RRR PPM (i = 1, 2, and 3 in this study); the distance a between the hinge axes A_1 and A_2; the distance b between the hinge axes A_2 and A_3; the distance c between the hinge axes A_3 and A_1; and the lengths d, e, and f of the three sides of the moving platform triangle $C_1C_2C_3$. Based on the above conditions, the following values can be obtained: the global coordinates (x_{Ai}, y_{Ai}) of the points A_i and the global coordinates (x_{Ci}, y_{Ci}) and local coordinates (x_{Ci}', y_{Ci}') of the points C_i. The solving objective is the rotation angle θ_i of the rods A_iB_i [8].

According to the theory of mechanism and coordinate transformation relation between the global and local coordinate systems [8], the coordinates of the points C_i in the global coordinate system oxy are:

$$\begin{bmatrix} x_{Ci} \\ y_{Ci} \end{bmatrix} = \begin{bmatrix} x \\ y \end{bmatrix} + \begin{bmatrix} \cos\alpha & -\sin\alpha \\ \sin\alpha & \cos\alpha \end{bmatrix} \begin{bmatrix} x_{Ci}' \\ y_{Ci}' \end{bmatrix} \tag{1}$$

The coordinates of the points B_i in the global coordinate system oxy are:

$$\begin{bmatrix} x_{Bi} \\ y_{Bi} \end{bmatrix} = \begin{bmatrix} x_{Ai} + l_i\cos\theta_i \\ y_{Ai} + l_i\sin\theta_i \end{bmatrix} \tag{2}$$

The methods for solving (x_{Ai}, y_{Ai}), (x_{Ci}', y_{Ci}') based on the dimensional parameters a, b, c, d, e, and f of the 3-RRR PPM are provided in Eqs. (26) to (35) of **the Appendix** of a previous study [8].

Eq. (3) can be obtained based on vector algebra and the geometric relationship of the 3-RRR PPM [8].

$$M_i^2 + N_i^2 - 2M_il_i\cos\theta_i - 2N_il_i\sin\theta_i = {l_{i+3}}^2 - l_i^2 \tag{3}$$

where

$$M_i = x + x_{ci}'\cos\alpha - y_{ci}'\sin\alpha - x_{Ai} = x_{Ci} - x_{Ai} \tag{4}$$

$$N_i = y + x_{ci}'\sin\alpha + y_{ci}'\cos\alpha - y_{Ai} = y_{Ci} - y_{Ai} \tag{5}$$

The rotation angle θ_i of the active rods is expressed as:

$$\theta_i = 2\tan^{-1}\frac{N_i \pm \sqrt{N_i^2 + M_i^2 - K_i^2}}{M_i + K_i} \tag{6}$$

where

$$K_i = \frac{M_i^2 + N_i^2 + l_i^2 - {l_{i+3}}^2}{2l_i} \tag{7}$$

Furthermore, the condition that Eq. (6) has a real number solution is expressed by Eq. (8) as follows:

$$N_i^2 + M_i^2 \geq K_i^2 \tag{8}$$

2.2 AMs for the 3-RRR PPM

The AMs of the 3-RRR PPM are also referred to as working modes [7, 8, 23]. For "±" in the numerator of Eq. (6), either "+" or "−" can be selected. Based on the principles of combinatorics, eight different inverse solutions corresponding to eight AMs are listed as follows (θ_i^+ expresses "+" in the numerator "±" and θ_i^- expresses "−" in Eq. (6)): (i) θ_1^+, θ_2^+, and θ_3^+ (+++ AM); (ii) θ_1^+, θ_2^-, and θ_3^- (+−−AM); (iii) θ_1^+, θ_2^+, and θ_3^- (++− AM); (iv) θ_1^+, θ_2^-, and θ_3^+ (+−+ AM); (v) θ_1^-, θ_2^+, and θ_3^+ (−++ AM); (vi) θ_1^-, θ_2^-, and θ_3^- (−−− AM); (vii) θ_1^-, θ_2^+, and θ_3^- (−+− AM); and (viii) θ_1^-, θ_2^-, and θ_3^+ (−−+AM).

It must be noted that if there is no overlapping area in the motion range of the active rods related to the different AMs, online conversion of the AMs is not feasible. Only if the 3-RRR PPM is disassembled and subsequently reassembled, a particular type of AM can be converted into another type of AM [8].

2.3 Definition of Singularity and Singularity-Free Workspace

Eqs. (9) to (11) can be obtained by differentiating the two sides of Eqs. (3) to (5) with respect to time [8].

$$\dot{M}_i = \dot{x} - \dot{\alpha}\,x_{ci}'\sin\alpha - \dot{\alpha}\,y_{ci}'\cos\alpha \tag{9}$$

$$\dot{N}_i = \dot{y} + \dot{\alpha} x_{ci}' \cos\alpha - \dot{\alpha} y_{ci}' \sin\alpha \tag{10}$$

$$\begin{aligned} &\left(l_i \cos\theta_i - M_i\right)\dot{M}_i + \left(l_i \sin\theta_i - N_i\right)\dot{N}_i = \\ &= l_i\left(M_i \sin\theta_i - N_i \cos\theta_i\right)\dot{\theta}_i \end{aligned} \tag{11}$$

Based on Eqs. (9) to (11), Eq. (12) can be obtained as follows:

$$\boldsymbol{\Phi}_y \begin{bmatrix} \dot{x} \\ \dot{y} \\ \dot{\alpha} \end{bmatrix} = \boldsymbol{\Phi}_z \begin{bmatrix} \dot{\theta}_1 \\ \dot{\theta}_2 \\ \dot{\theta}_3 \end{bmatrix} \tag{12}$$

where the diagonal matrix $\boldsymbol{\Phi}_z$ is called the discriminant matrix of the first type of singularity [7, 8, 25] and can be expressed in the following form:

$$\boldsymbol{\Phi}_z = \begin{bmatrix} l_1(M_1 sin\theta_1 - N_1 cos\theta_1) & 0 & 0 \\ 0 & l_2(M_2 sin\theta_2 - N_2 cos\theta_2) & 0 \\ 0 & 0 & l_3(M_3 sin\theta_3 - N_3 cos\theta_3) \end{bmatrix} \tag{13}$$

The matrix $\boldsymbol{\Phi}_y$ is called the discriminant matrix of the second type of singularity [7, 8, 25] and can be expressed in the following form:

$$\boldsymbol{\Phi}_y = \begin{bmatrix} l_1\cos\theta_1 - M_1 & l_1\sin\theta_1 - N_1 & \left(l_1\sin\theta_1 - N_1\right)\left(M_1 + x_{A1} - x\right) - \left(l_1\cos\theta_1 - M_1\right)\left(N_1 + y_{A1} - y\right) \\ l_2\cos\theta_2 - M_2 & l_2\sin\theta_2 - N_2 & \left(l_2\sin\theta_2 - N_2\right)\left(M_2 + x_{A2} - x\right) - \left(l_2\cos\theta_2 - M_2\right)\left(N_2 + y_{A2} - y\right) \\ l_3\cos\theta_3 - M_3 & l_3\sin\theta_3 - N_3 & \left(l_3\sin\theta_3 - N_3\right)\left(M_3 + x_{A3} - x\right) - \left(l_3\cos\theta_3 - M_3\right)\left(N_3 + y_{A3} - y\right) \end{bmatrix} \tag{14}$$

The first type of singularity occurs if $\det(\boldsymbol{\Phi}_z) = 0$ and the second type of singularity occurs if $\det(\boldsymbol{\Phi}_y) = 0$. The third type of singularity occurs if $\det(\boldsymbol{\Phi}_z) = 0$ and $\det(\boldsymbol{\Phi}_y) = 0$ [7, 8, 25]. Therefore, the condition in which there is no singularity can be expressed by Eq. (15):

$$\begin{cases} \left|\det\left(\boldsymbol{\Phi}_y\right)\right| > 0 \\ \left|\det\left(\boldsymbol{\Phi}_z\right)\right| > 0 \end{cases} \tag{15}$$

For different orientation angles of the moving platform and different AMs, under the premise of satisfying Eqs. (8) and (15), the non-singular position workspace of the 3-RRR PPM can be determined by a two-dimensional search method, namely, the set of points (x, y) [8].

2.4 Further Discussion for the First and Second Type of Singularity

2.4.1 The Sufficient Condition of the First Type of Singularity for the 3-RRR PPM and the Probable Distribution of the First Type of Singularity in the Workspace

As shown in Fig. 1, in any branch chain of the 3-RRR PPM, if the active rod A_iB_i and passive rod B_iC_i are straightened or overlapped on the same straightline, then $\det(\boldsymbol{\Phi}_z) = 0$; that is, there must be the first singular phenomenon [15-17].

The above-mentioned sufficient condition of the first type of singularity is proved in the **Appendix A** through linear algebra [26]. Based on this, in general, if the condition that the active and passive rods in the same branch chain are straightened or overlapped on the same straight line is true, it can be seen that the first type of singularity appears at the limit position of the active rod; that is, the first-type singular points may appear near the boundary of the workspace. On the contrary, if the condition that the active and passive rods in the same branch chain are straightened or overlapped on the same straightline is geometrically impossible, the boundary points of the workspace are not necessarily the first-type singular points.

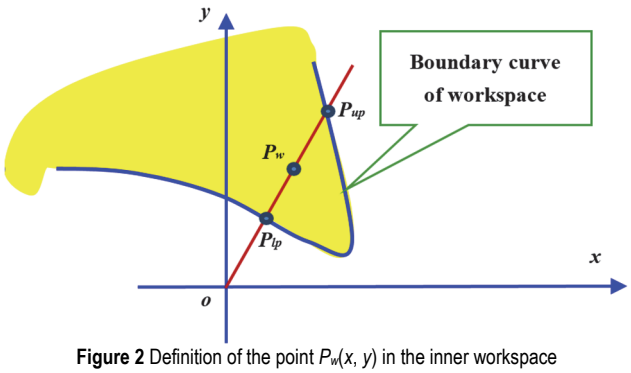

Figure 2 Definition of the point $P_w(x, y)$ in the inner workspace

The boundary points of the work space corresponding to any type of AM or the given orientation α of the moving platform are much more likely to fall outside the workspace when the AM or the given orientation α of the moving platform is changed. Therefore, the boundary points of the workspace must be excluded when the AM conversion for singularity avoidance is implemented. That is, without considering the first and third types of singularity in the boundary of the workspace, in the polar coordinate system shown in Fig. 2, according to the distance between the point $P_w(x, y)$ in the workspace and upper boundary point $P_{up}(x_{up}, y_{up})$ or lower boundary point $P_{lp}(x_{lp}, y_{lp})$, the point that satisfies Eq. (16) is defined as the point $P_w(x, y)$ in the inner workspace.

$$\begin{cases} \sqrt{(x-x_{up})^2+(y-y_{up})^2} \geq \dfrac{1}{\rho}\sqrt{(x_{up}-x_{lp})^2+(y_{up}-y_{lp})^2} \\ \sqrt{(x-x_{lp})^2+(y-y_{lp})^2} \geq \dfrac{1}{\rho}\sqrt{(x_{up}-x_{lp})^2+(y_{up}-y_{lp})^2} \end{cases} \tag{16}$$

where $\rho \in [10^3, 10^4]$ is a constant and the lower or upper limiting value corresponds to a wider or narrower workspace boundary. When searching for the singularity-free workspace of the 3-RRR PPM, the boundary and its nearby points that do not satisfy the condition of Eq. (16) are allowed to have the first, second, and even third types of singularity. The boundary and its nearby points are excluded, and the singularity-free condition for the 3-RRR PPM is changed from Eq. (15) to

$$\left|\det\left(\boldsymbol{\Phi}_y\right)\right| > 0 \tag{17}$$

For convenience, $z = \det(\boldsymbol{\Phi}_y)$ is called the discriminant surface of the second type of singularity, and the intersection curve of the spatial surface $z = \det(\boldsymbol{\Phi}_y)$ and the workspace plane $z = 0$ is called the curve of the second type of singularity.

2.4.2 The Necessary and Sufficient Condition of the Second Type of Singularity for the 3-RRR PPM

The second type of singularity occurs for the 3-RRR PPM if and only if the three different straight lines that belong to the passive rods B_1C_1, B_2C_2, and B_3C_3 are concurrent or parallel, or any two of the three straight lines B_1C_1, B_2C_2, and B_3C_3 are parallel and collinear [8, 15-17]. Where, the three different straight lines mean that no two of the three lines coincide on the same straight line.

And the above-mentioned necessary and sufficient condition of the second type of singularity is proved in the **Appendix B** through linear algebra [26].

An important implication can be inferred from the above-mentioned condition, that is, the geometric conditions of the second type of singularity are no longer satisfied once the AMs are changed.

3 METHOD TO AVOID THE SECOND TYPE OF SINGULARITY BASED ON OFF LINE CONVERSION OF AMs FOR THE 3-RRR PPM

3.1 Geometric Principle to Avoid the Second Type of Singularity through Conversion of AMs

In general, based on the necessary and sufficient condition of the second type of singularity for the 3-RRR PPM, special geometric relations among the passive rods B_iC_i are satisfied when the second type of singularity arises for the 3-RRR PPM, whereas the passive rods B_iC_i do not meet the three geometric conditions in the necessary and sufficient condition of the second type of singularity for the 3-RRR PPM, and the position and orientation of the second type of singularity are eliminated. Therefore, there are two ways to avoid the second type of singularity by changing the position of the points C_i or B_i.

(1) Orientation perturbation of moving platform to avoid singularity: This is a method to avoid singularity without changing the centroid position of the moving platform and only changing the orientation angle of the moving platform. The geometric principle of this method is to change the position of the points C_i when the singularity of the manipulator arises, which is reported in a previous study [8] and is not repeated here.

(2) Changing the AMs to avoid singularity: This method does not change the orientation angle and position coordinates of the centroid of the moving platform but only changes the AMs. The geometric principle is to change the position of the points B_i when the singularity of the manipulator arises such that the three geometric conditions in the necessary and sufficient condition of the second type of singularity for the 3-RRR PPM are no longer satisfied among the passive rods B_iC_i.

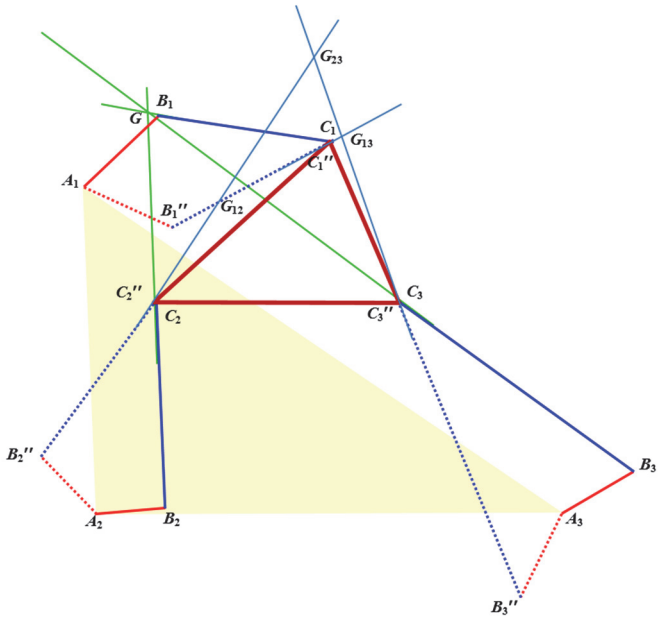

(a) Three different straight lines *BiCi* intersect at point *G*

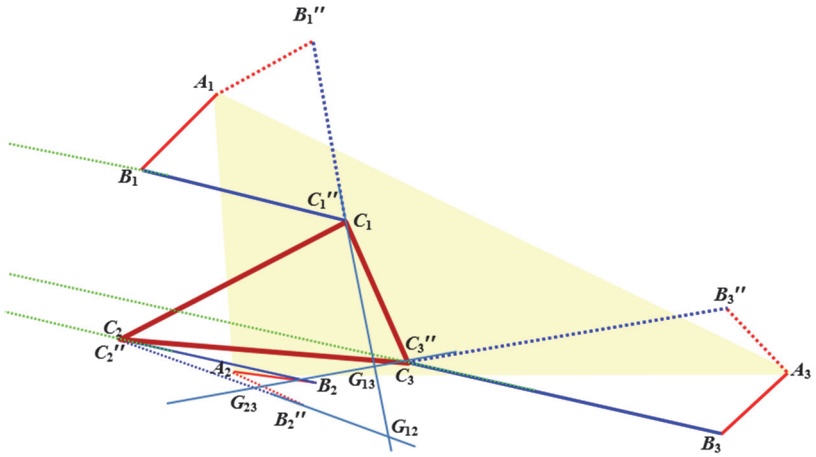

(b) Three different straight lines *BiCi* are parallel to each other

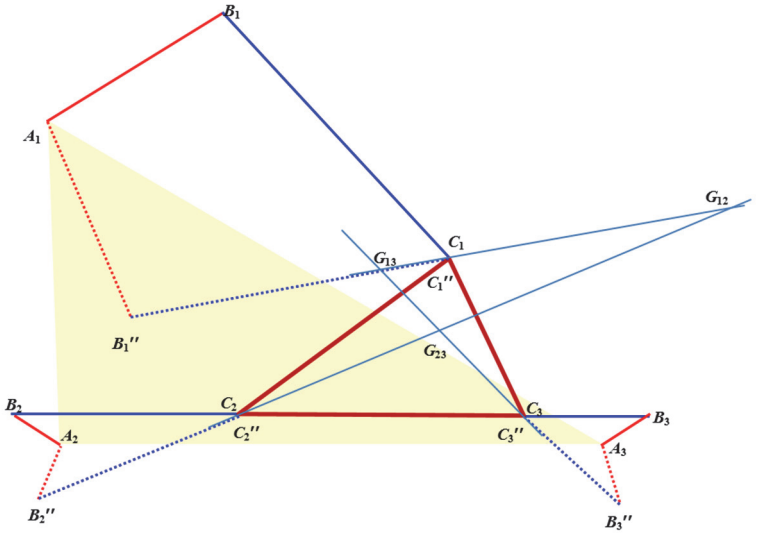

(c) Two of the three straight lines *BiCi* are parallel and collinear

Figure 3 Geometric principle to avoid the singularity through conversion of AMs

According to Eqs. (2) and (6), the geometric positions of active rods A_iB_i corresponding to the AMs are as follows (Fig. 3a to c): In the "+" mode, the coordinates of the points B_i are $(x_{Ai}+l_i\cos\theta_i^+, y_{Ai}+l_i\sin\theta_i^+)$; when the assembly mode is changed to the "−" mode, the points B_i reach the new position B_i'' whose coordinates are $(x_{Ai}+l_i\cos\theta_i^-, y_{Ai}+l_i\sin\theta_i^-)$. The heavy lines correspond to the singular position of the 3-RRR PPM, and the fine dotted lines correspond to the new position after changing the AMs. Because the centroid position and orientation of the moving platform are not changed, the straight lines B_iC_i reach the new position $B_i''C_i''$ (C_i and C_i'' are the coincident points).

And $A_iB_i = A_iB_i''$, $B_iC_i = B_i''C_i''$, $B_iB_i''\perp A_iC_i$, and $B_iB_i''\perp A_iC_i''$. Therefore, after the AMs are changed, B_iC_i takes A_iC_i (or A_iC_i'') as the axis of symmetry and rotates around the points C_i (or C_i'') to a new position $B_i''C_i''$.

In Fig. 3a, the three different straight lines B_iC_i are concurrent at point G. Because B_iC_i has rotated an angle around the points C_i (or C_i''), the three new straight lines $B_i''C_i''$ are no longer concurrent but intersect at points G_{12}, G_{23}, and G_{13}, respectively.

Similarly, in Fig. 3b, the three different straight lines B_iC_i are parallel to each other, but after changing the AMs, the new position $B_i''C_i''$ of the three straight lines B_iC_i no longer satisfies the geometric conditions of being parallel to each other.

As shown in Fig. 3c, B_2C_2 and B_3C_3 are parallel and collinear. After changing the AMs, the geometric conditions of the second type of singularity are no longer satisfied.

3.2 Problem Statement and Program Implementation of Offline Conversion of AMs for Avoiding the Second Type of Singularity

If the dimensional parameters of the 3-RRR PPM are given, under eight different AMs, how does one determine the total inner singularity-free workspace that simultaneously satisfies Eqs. (16) and (17) and the range $\alpha\in[\alpha_s, \alpha_e]$ of the orientation angle of the moving platform? That is, if Eq. (16) is not satisfied (i.e. the points are at or near the workspace boundary), how does one determine the AM and range $\alpha\in[\alpha_s, \alpha_e]$ of the orientation angle of the moving platform corresponding to the inner singularity-free workspace?

When the point set of the position workspace for the 3-RRR PPM is not empty, the ranges $\alpha\in[-\alpha_{01}, \alpha_{02}]$ of the orientation angle of the moving platform can be defined such that $\alpha_{01}, \alpha_{02} \geq 0$. At the same time, the possible constant-orientation workspace, that is, the search area can be

expressed by Eq. (18) [8].

$$\begin{cases} x = r\cos\theta \\ y = r\sin\theta \end{cases} \tag{18}$$

where (x, y) are the centre-of-mass coordinates of the moving platform, r is the radius of the searched circle, and the value ranges of r and θ are [0, R] and [0, 2π], respectively [8].

As shown in Fig. 4, the eight subprograms corresponding to the eight different AMs are developed to search for the required workspace in which there is no second type of singularity for the 3-RRR PPM.

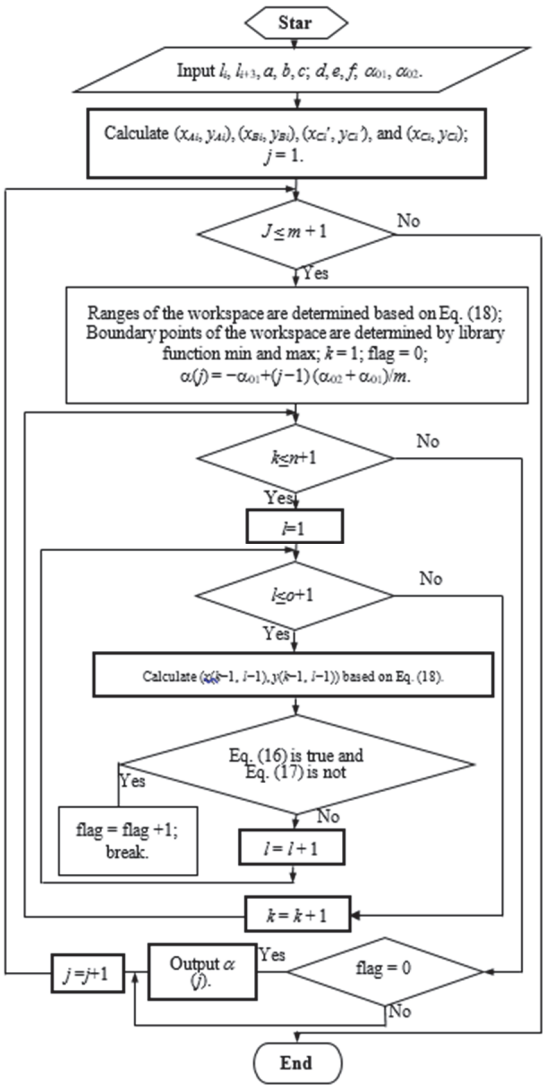

Figure 4 Program flowchart to determine the ranges of the orientation angle of the moving platform corresponding to singularity-free inner workspace under the given AM

The development idea of these subprograms is the same and is based on three layers of for-loop nesting as follows:

The first (outermost) layer for-loop with loop variable $j \in [1, m + 1]$ is used, where $m \cdot \Delta\alpha = \alpha_{02}+\alpha_{01}$ and $\alpha(j) = -\alpha_{01} + (j - 1)(\alpha_{02} + \alpha_{01})/m$; the second layer for-loop with loop variable $k \in [1, n + 1]$ is used, where $k \cdot \Delta r = R$; and the third (innermost) layer for-loop with loop variable $l \in [1, o + 1]$ is used, where $l \cdot \Delta\theta = 2\pi$. It should be noted that m, k, and l are positive integers.

In the body of the outermost layer for-loop, the ranges of the workspace based on equation (34) are determined by a two-dimensional search, and then the boundary points of the workspace are determined by library functions min and max [8]. On this basis, first, the variable flag is assigned as 0; subsequently, the second and third layer for-loops are executed once again; next, in the body of the innermost layer for-loop, the conditions that Eq. (16) is true and Eq. (17) is not are estimated by the if statement: if the conditions are satisfied, the variable flag is assigned as flag + 1, and in the meantime, the program is terminated out of the innermost layer for-loop by the break statement. Finally, when the outermost layer for-loop ends everytime, whether the variable flag is equal to 0 or not is estimated by the if statement: $\alpha(j)$ is the output if the variable flag is equal to 0, where $\alpha(j) = -\alpha_{01} + (j - 1)(\alpha_{02} + \alpha_{01})/m$ and the program continues in sequence if the variable flag is not equal to 0.

3.3 Example, Analysis and Experimental Verification

3.3.1 Example and Results Analysis

As shown in Fig. 1, the dimensional parameters for the 3-RRR PPM are selected as follows: The lengths a, b, and c of the sides of the triangle $A_1A_2A_3$ are 53.1, 91.9, and 108.3 (length unit: mm), respectively; the lengths d, e, and f of the sides of the triangle $C_1C_2C_3$ are 43.9, 48.1, and 28.9, respectively; the lengths l_1, l_2, and l_3 of the active rods A_iB_i are 19, 14, and 16, respectively; and the lengths l_4, l_5, and l_6 of the passive rods B_iC_i are 35, 34, and 54, respectively.

Inside the workspace, except for the points at or near the boundary, the variation range of the orientation angle of the moving platform and the corresponding AMs without the second-type singular points are obtained as follows:

When the orientation angle α of the moving platform belongs to the ranges [−360°, −30°] and [60°, 360°], the corresponding position workspace either does not exist, degenerates to a point, or the range is very small; therefore, there is no value for engineering applications and discussions. Thus, the available workspace of α∈[−30°, 60°] is searched using eight subprograms corresponding to the eight different AMs, according to the flow chart in illustrated Fig. 4; $\rho = 1000$ is considered, and the developed program is run.

Under the "−−+" AM, when α∈[−5.5°, 11°], there are no second-type singular points in the workspace except the points at or near the boundary. In the interval α∈[−5.5°, 11°], the orientation angles α = −5.5°, −3.5°, 0°, 5°, 8° and 11° are selected, and the spatial position relationship between the workspace (shown in yellow) and the spatial surface (shown in blue) of $z = \det(\boldsymbol{\Phi}_y)$ is displayed in the same three-dimensional coordinate system, as shown in Fig. 5a (l), where Fig. 5b, d, f, h, j, and l are the three-dimensional space graphics and Fig. 5a, c, e, g, i, and k are the projections of the corresponding three-dimensional space graphics in the workspace plane $z = 0$.

As a supplement to and for a comparative analysis of the above results, the following three cases are noteworthy.

Case 1. Under the "−−+" AM, when $\alpha \in [-5.5°, 11°]$, the boundary points that do not satisfy Eq. (21), such as the boundary points P_{B1} - P_{B6}, as shown in Fig. 5a, c, e, g, i, and k, and the corresponding position and orientation for the 3-RRR PPM are the first-type singular points or close to them; at the intersection of the boundary points and the curve of the second type of singularity, the corresponding position and orientation for the 3-RRR PPM are the third type or close to third type of singularities.

The position and orientation of the 3-RRR PPM corresponding to the boundary points P_{B1} - P_{B6} in Fig. 5a, c, e, g, i, and k are shown in Fig. 6a to f.

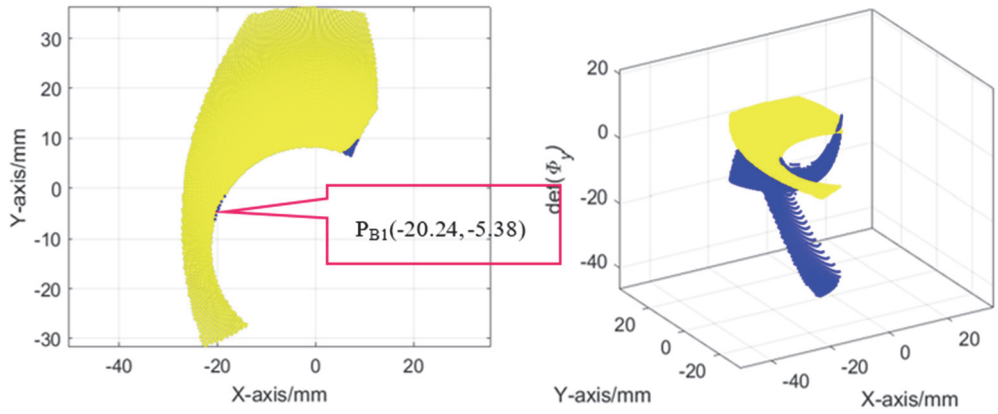

(a) and (b) $\alpha = -5.5°$

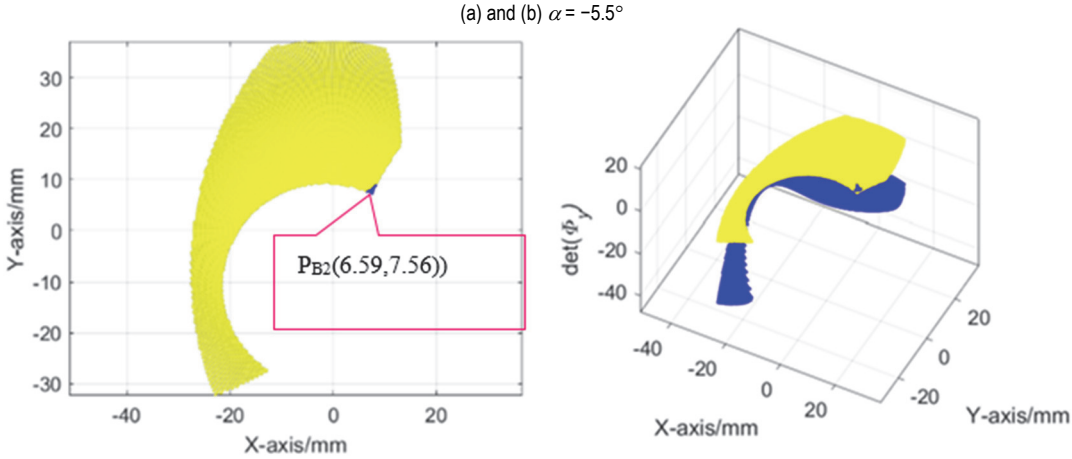

(c) and (d) $\alpha = -3.5°$

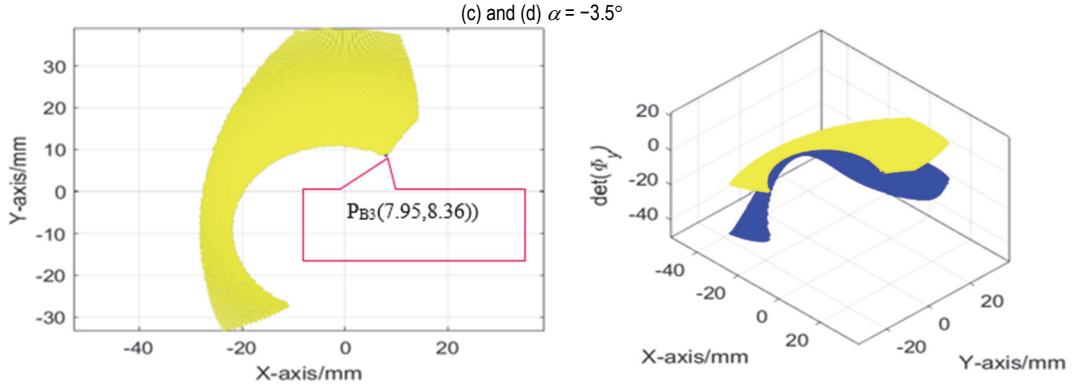

(e) and (f) $\alpha = 0°$

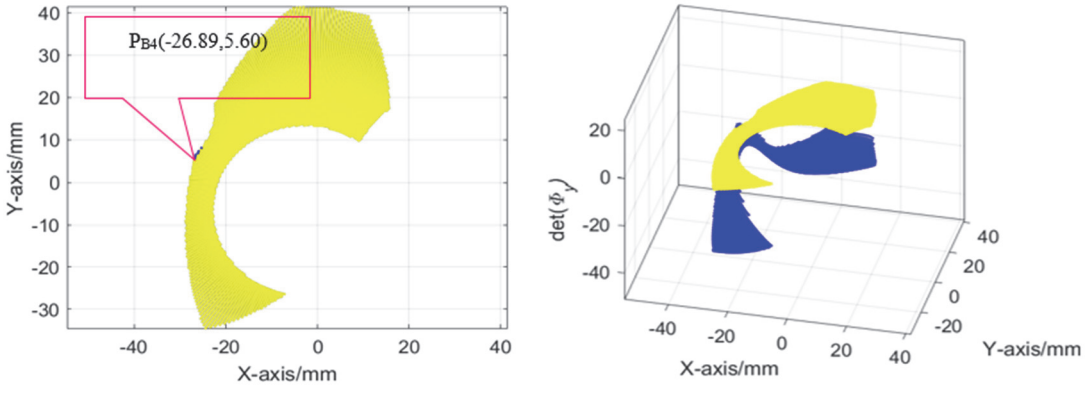

(g) and (h) $\alpha = 5°$

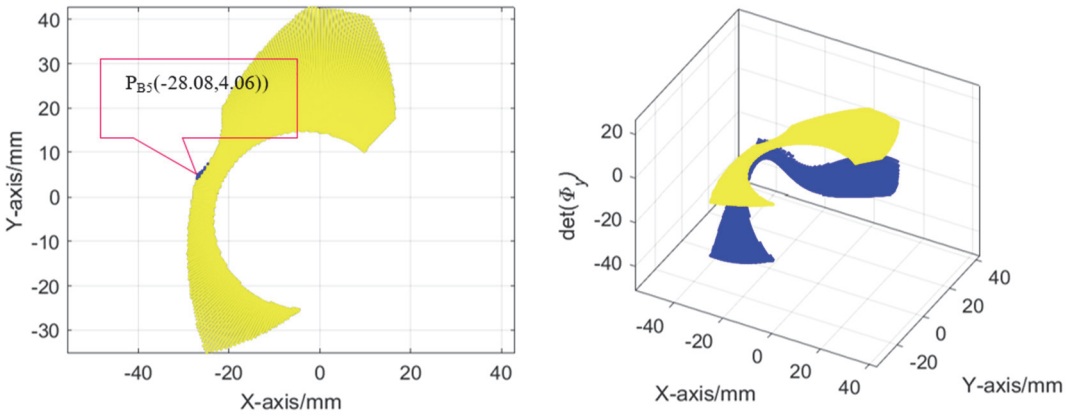

(i) and (j) $\alpha = 8°$

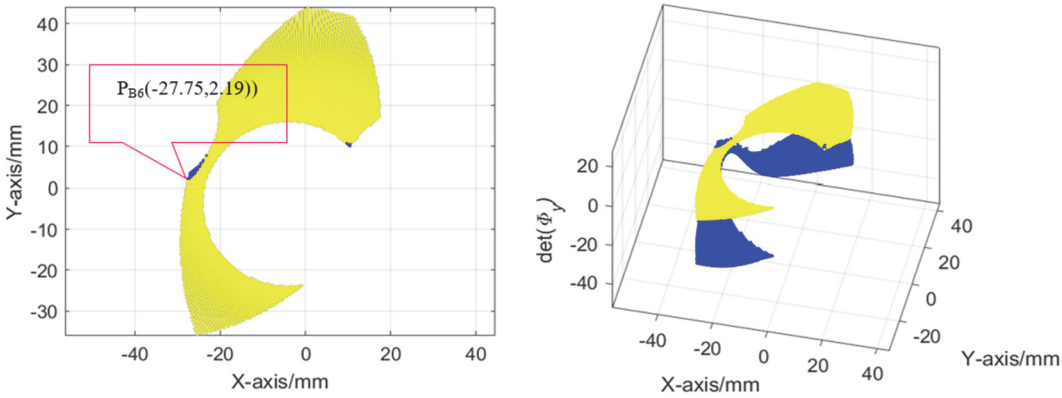

(k) and (l) $\alpha = 11°$

Figure 5 Workspace without the second-type singular points except at the boundary under "−−+" AM when $\alpha \in [-5.5°, 11°]$

In Fig. 6a, when $\alpha = -5.5°$ and the centroid of the moving platform is at the boundary point P_{B1} (−20.24 mm, −5.38 mm), A_2B_2 and B_2C_2 overlap on the same straight line and B_1C_1,B_2C_2, and B_3C_3 are parallel to each other; thus, there is a third type of singularity.

In Fig. 6b, when $\alpha = -3.5°$ and the centroid of the moving platform is at the boundary point P_{B2} (6.59 mm, 7.56 mm), A_2B_2 and B_2C_2 overlap on the same straight line, and B_1C_1, B_2C_2, and B_3C_3 are concurrent; thus, there is a third type of singularity.

In Fig. 6c, when $\alpha = 0°$ and the centroid of the moving platform is at the boundary point P_{B3} (7.95 mm, 8.36 mm), A_2B_2 and B_2C_2 overlap on the same straight line; thus, there is a first type of singularity.

In Fig. 6d, when $\alpha = 5°$ and the centroid of the moving platform is at the boundary point P_{B4} (−26.89 mm, 5.60 mm), A_3B_3 and B_3C_3 are straightened on the same straightline; thus, there is a first type of singularity.

In Fig. 6e, when $\alpha = 8°$ and the centroid of the moving platform is at the boundary point P_{B5} (−28.08 mm, 4.06 mm), A_3B_3 and B_3C_3 are straightened on the same straightline; thus, there is a first type of singularity.

In Fig. 6f, when $\alpha = 11°$ and the centroid of the moving platform is at the boundary point P_{B6} (−27.75 mm, 2.19 mm), A_3B_3 and B_3C_3 are straightened on the same straightline and B_1C_1, B_2C_2, and B_3C_3 are concurrent; thus, there is a third type of singularity.

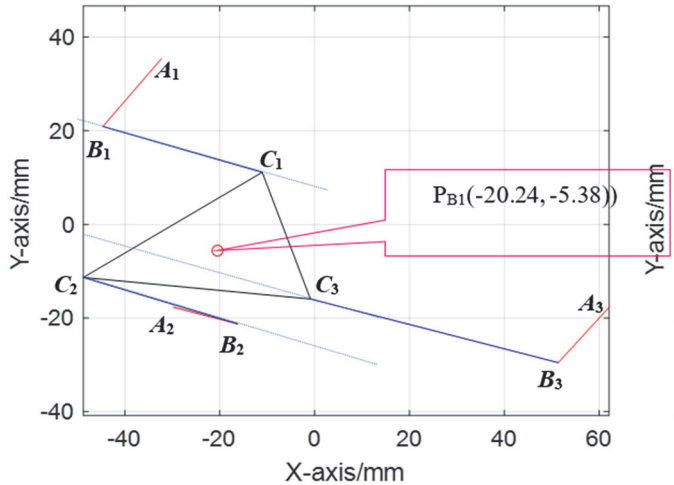

(a) $\alpha = -5.5°$, P_{B1} (−20.24, -5.38)

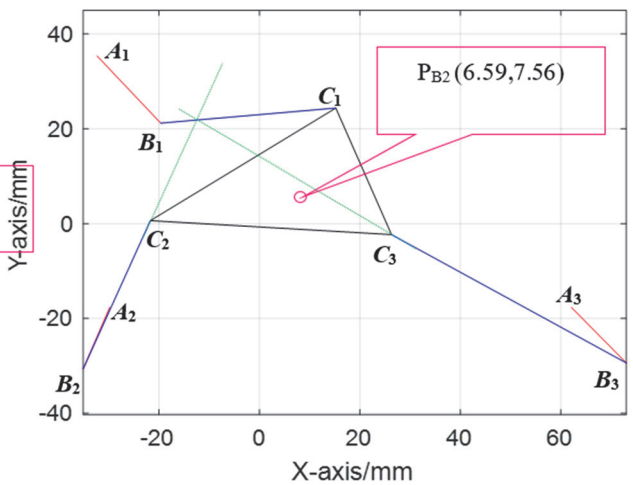

(b) $\alpha = -3.5°$, P_{B2} (6.59, 7.56)

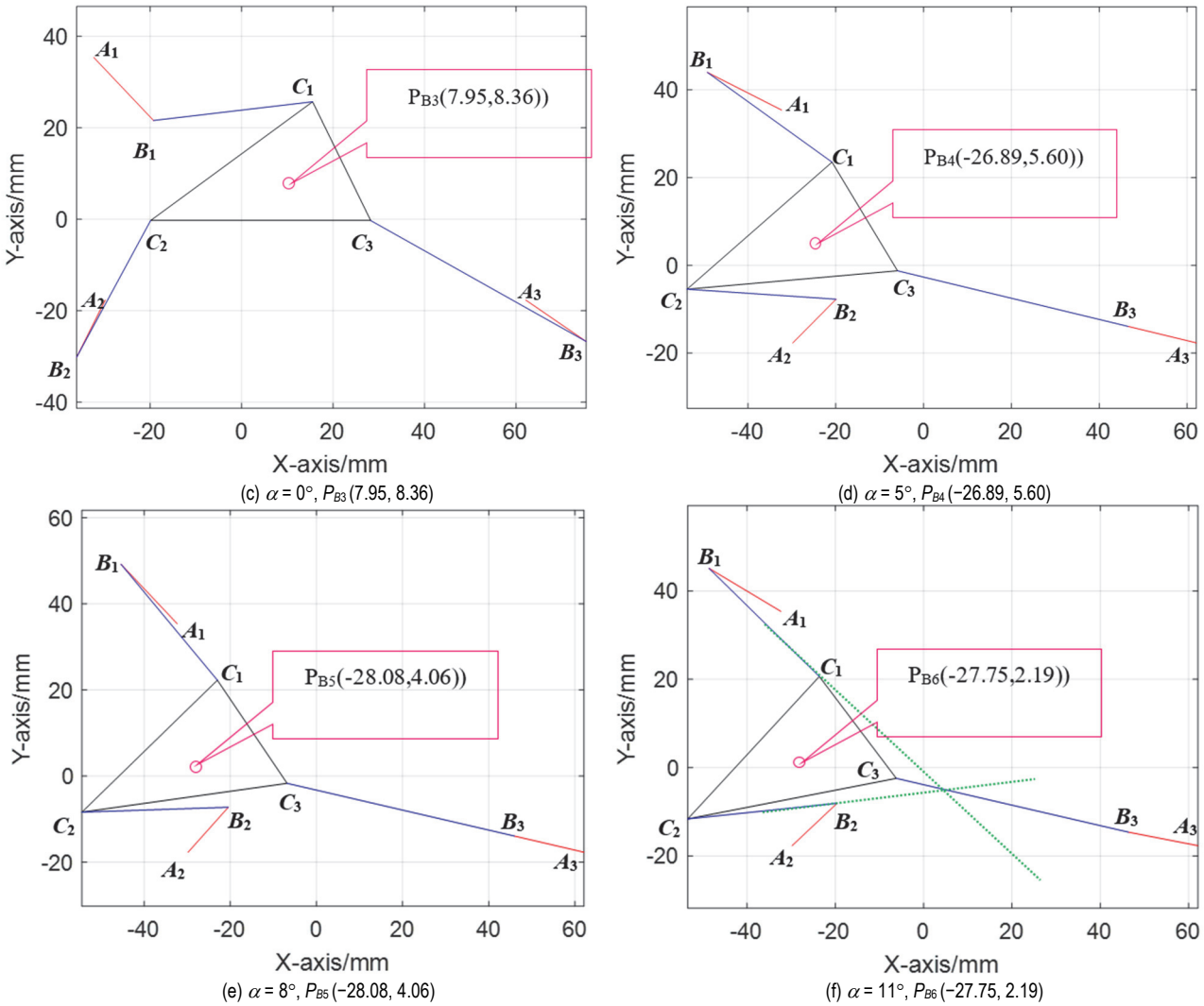

(c) $\alpha = 0°$, P_{B3} (7.95, 8.36)
(d) $\alpha = 5°$, P_{B4} (−26.89, 5.60)
(e) $\alpha = 8°$, P_{B5} (−28.08, 4.06)
(f) $\alpha = 11°$, P_{B6} (−27.75, 2.19)

Figure 6 The position and orientation for the 3-RRR PPM corresponding to the boundary points P_{B1} - P_{B6} under "−−+" AM when $\alpha \in [-5.5°, 11°]$

Case 2. Under the **"−−+"** AM, when $\alpha \in [-30°, -5.5°]$ and $\alpha \in [11°, 60°]$, there are no inner workspaces that do not have the second-type singular points, except for the points at or near the boundary, for the 3-RRR PPM. Furthermore, $\alpha = -15°, -8°, 15°$ and $20°$ are selected, and the projections of the corresponding workspace plane and discriminant surface of the second type of singularity $z = \det(\boldsymbol{\Phi}_y)$ on the *xoy* coordinate plane are given. The curve of the second type of singularity and distribution of the singular points in the workspace are shown in Fig. 7a to d.

Case 3. Under the "+++", "+−+", "−++", "++−", "+−−", "−+−" and "−−−" AMs (seven different AMs that exclude the "−−+" AM), when $\alpha \in [-30°, 60°]$, there are no inner workspaces that do not have the second-type singular points except for the points at or near the boundary for the 3-RRR PPM. $\alpha = 5°$ is selected, and the projections of the corresponding workspace plane and spatial surface $z = \det(\boldsymbol{\Phi}_y)$ on the *xoy* coordinate plane are given. The curve of the second type of singularity and distribution of the singular points in the workspace are shown in Fig. 8a to g.

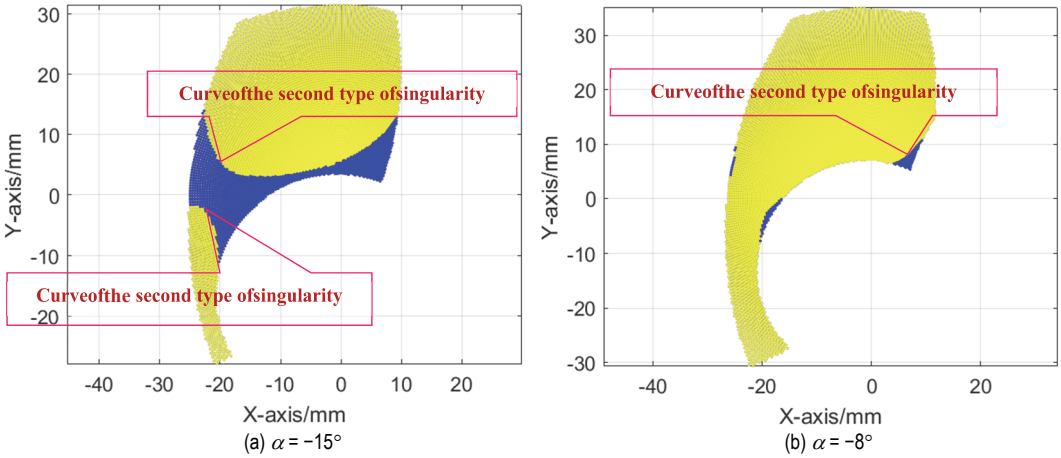

(a) $\alpha = -15°$
(b) $\alpha = -8°$

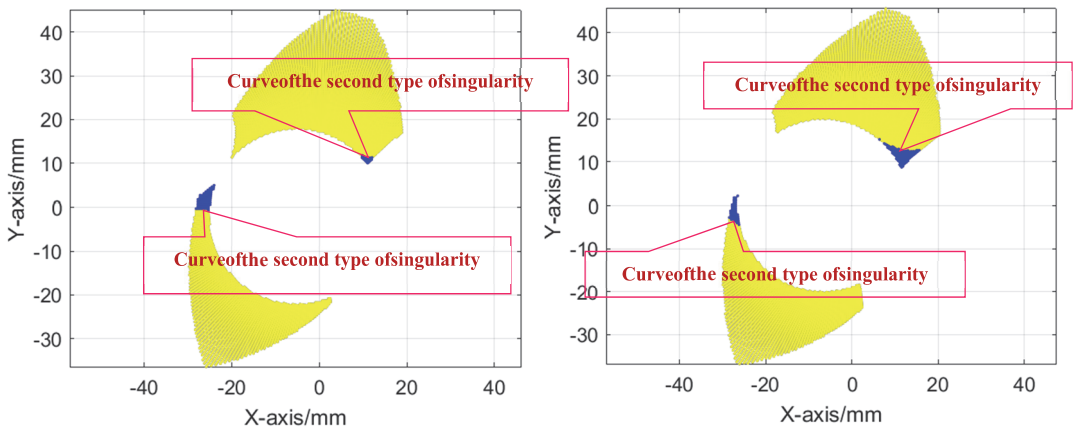

(c) $\alpha = 15°$ (d) $\alpha = 20°$

Figure 7 The second type of singularity in the workspace of the 3-RRR PPM under "−−+" AM when $\alpha \in [-30°, -5.5°]$ and $\alpha \in [11°, 60°]$

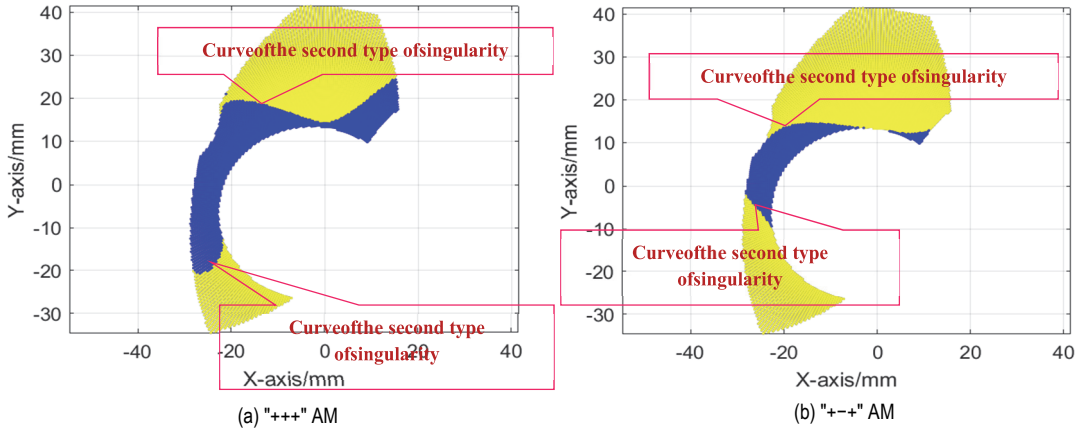

(a) "+++" AM (b) "+−+" AM

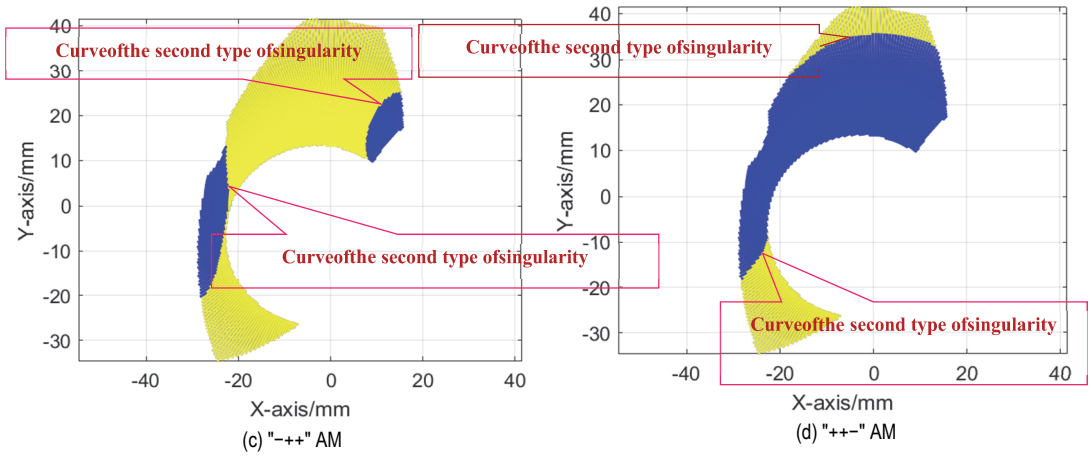

(c) "−++" AM (d) "++−" AM

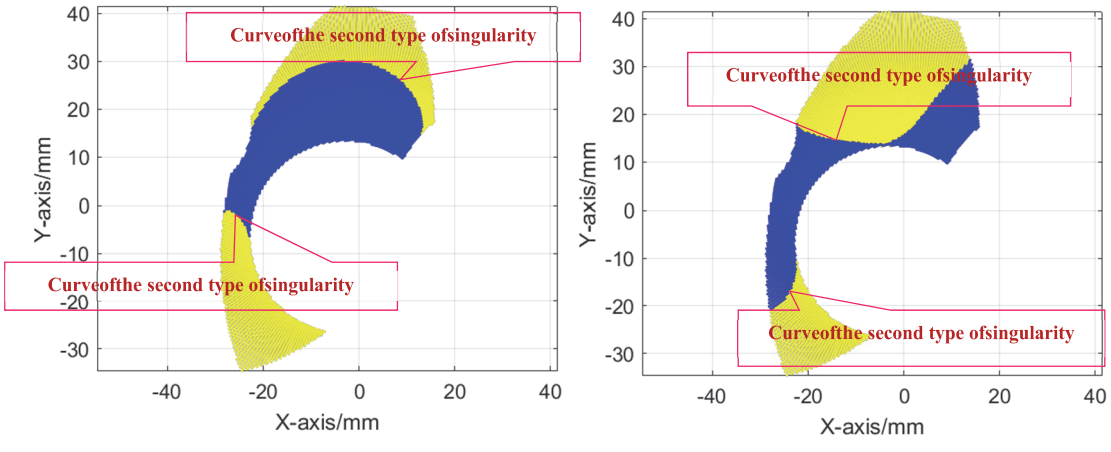

(e) "+−−" AM (f) "−+−" AM

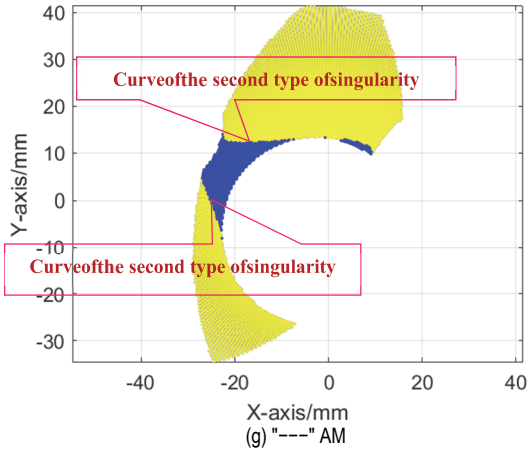

(g) "−−−" AM

Figure 8 The second type of singularity in the workspace of the 3-RRR PPM excluding the "−−+" AM when $\alpha = 5°$

Therefore, among the eight different AMs of the 3-RRR PPM, only the "−−+" AM satisfies the condition of no second-type singular points in the inner workspace while simultaneously satisfying Eq. (21) when $\alpha \in [-5.5°, 11°]$, except for the points at or near the boundary.

3.3.2 Experimental Verification

As depicted in Fig. 9, to verify the validity of the proposed method, a testing system based on field bus technology was integrated, after the mechanical system of the 3-RRR PPM was manufactured [8].

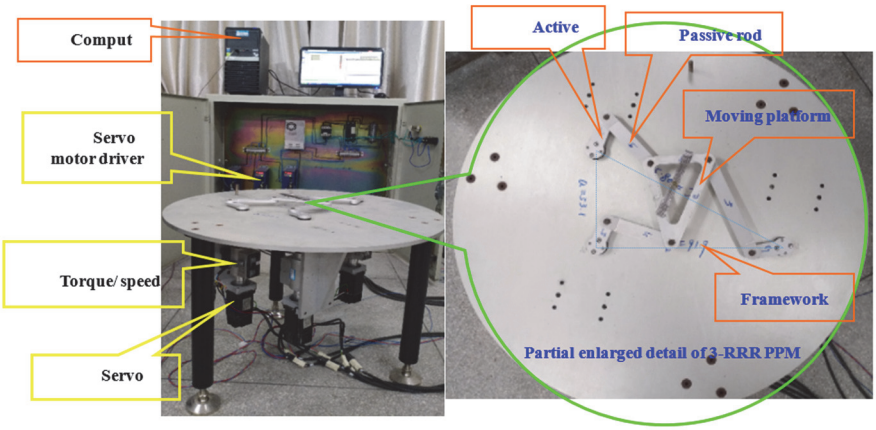

Figure 9 Testing system

The integrated system is composed of the mechanical subsystem of the 3-RRR PPM, three torque/speed sensors (signal detection subsystem), and a servo control subsystem, that includes three servo motors, three servo motor drivers, and a computer [8].

Under the "−−+" AM, different orientation angles of the moving platform correspond to different workspace ranges. A task path is planned when the common area of the workspace $\alpha \in [-5.5°, 11°]$ is considered, with a total movement time of T = 15 s. The centroid (x, y) of the moving platform varies with time according to Eq. (19), and the orientation angle $\alpha \in [-0.096$ rad, 0.192 rad] ($[-5.5°, 11°]$) of the moving platform varies with time according to Eq. (20).

$$\begin{cases} x = 9\left(1-\dfrac{t}{15}\right)\cos(\omega\pi t) \\ y = 26+9\left(1-\dfrac{t}{15}\right)\sin(\omega\pi t) \end{cases} \quad t \in [0,T] \tag{19}$$

$$\alpha = \frac{\pi}{180}(-5.5+1.1t) \quad t \in [0,T] \tag{20}$$

The inverse displacements of the 3-RRR PPM are calculated according to Eqs. (19) and (20). The relationship between the angular displacements θ_i of the active rods generated by Eq. (6) and the movement time t is shown in Fig. 10.

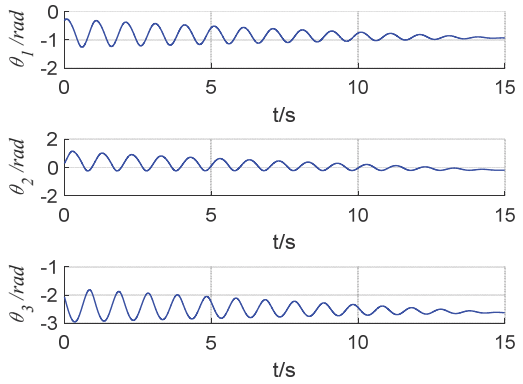

Figure 10 The relationship between the angular displacements θ_i of the active rods and movement time t

The initial angular displacements of the active rods are: $\theta_1 = -0.3183$ rad (−18.24°), $\theta_2 = 0.2811$ rad (16.11°), and $\theta_3 = -2.0635$ rad (−118.23°). To reveal the second type of singularity of the points on the planning path of Eq. (19), in the same coordinate system, the points $(x, y, 0)$ (denoted by yellow) corresponding to Eq. (19) and the points corresponding to $(x, y, \det(\boldsymbol{\Phi}_y))$ (denoted by blue) are shown in Fig. 11 by a scatter diagram.

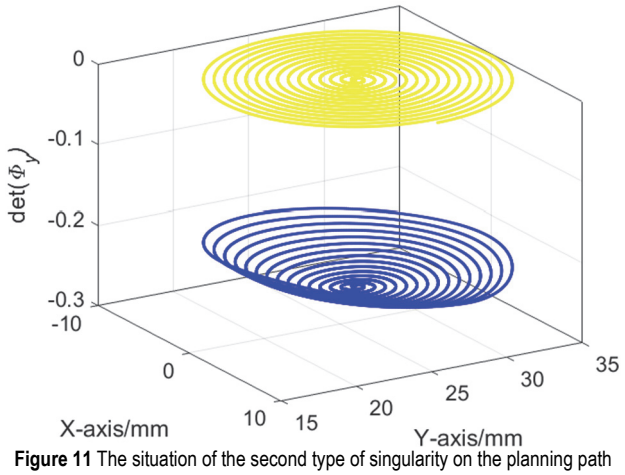

Figure 11 The situation of the second type of singularity on the planning path corresponding to Eq. (19)

Fig. 11 demonstrates that when the position and orientation of the moving platform change with time according to Eqs. (19) and (20), the value of the determinant $\det(\boldsymbol{\Phi}_y)$ is always less than 0, that is, there is no second-type singular phenomenon in the planning path.

After the 3-RRR PPM is installed and debugged according to the "−−+" AM, the initial angular displacements of the active rods are adjusted to $\theta_1 = -0.3183$ rad, $\theta_2 = 0.2811$ rad, and $\theta_3 = -2.0635$ rad. The testing system in Fig. 9 is commenced according to the motion law of the active rods in Fig. 10, and the experimental curve (shown in green) of the angular velocity of the active rods is generated based on the data of the speed sensor. Simultaneously, the simulation curve (shown in blue) of the angular velocity of the active rods is obtained by numerical differentiation of the data in Fig. 10. The comparative results of the simulation and experimental data for the angular velocity of the active rods are shown in Fig. 12.

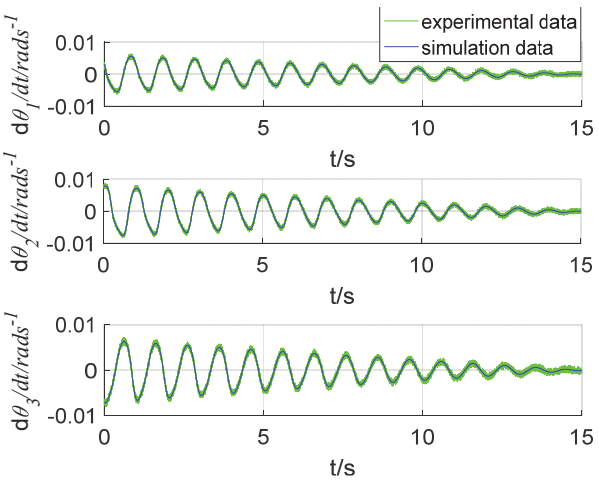

Figure 12 The comparative diagram between the simulation and experimental data of the angular velocity of the active rods

During the experiments, the singular phenomenon [8] was not observed in any of the three servo motors for the planned path corresponding to Eqs. (19) and (20). The experiment showed that inside the singular-free workspace, except for points that do not satisfy Eq. (16), the task path of the constant or variable orientation of the moving platform could be planned without any singularity.

4 CONCLUSION

The range of the orientation angle of the moving platform and the eight different AMs were comprehensively considered when the singular points at or near the boundary of the workspace were permitted. It was aimed at determining the condition for which the second-type singular points do not appear in the inner workspace, except for the points at or near the boundary. The AMs and ranges of the orientation angle of the moving platform corresponding to the inner singularity-free workspace are determined through a computer-based three-dimensional search method. The task path of the constant or variable orientation of the moving platform can be planned inside the singular-free inner workspace, and there is no singularity phenomenon.

Acknowledgments

The authors would like to thank the financial support of the National Natural Science Foundation of China (Grant No. 52005003) and the Major Natural Science Foundation of Anhui Provincial Universities (Grant Nos. GXXT-2019-021, and 2021cyxtb5) for their financial support.

5 REFERENCES

[1] Nag, A., Safar, V., & Bandyopadhyay, S. (2021). A uniform geometric-algebraic framework for the forward kinematic analysis of 6-6 Stewart platform manipulators of various architectures and other related 6-6 spatial manipulators. *Mechanism and Machine Theory*, *155*, 1-32. https://doi.org/10.1016/j.mechmachtheory.2020.104090

[2] Xie, Z., Li, G., Liu, G., & Zhao, J. (2017). Optimal design of a Stewart platform using the global transmission index under determinate constraint of workspace. *Advances in Mechanical Engineering*, *9*, 1-14. https://doi.org/10.1177%2F1687814017720880

[3] Szep, C., Stan, S. D., & Csibi, V. (2011). Design, workspace analysis and inverse kinematics problem of Delta parallel robot. *Mechanika*, *17*, 296-299. https://doi.org/10.5755/j01.mech.17.3.506

[4] Yong, Y. K. & Lu, T. F. (2009). Kinetostatic modeling of 3-RRR compliant micro-motion stages with flexure hinges. *Mechanism and Machine Theory*, *44*, 1156-1175. https://doi.org/10.1016/j.mechmachtheory.2008.09.005

[5] Saafi, H. & Lamine, H. (2020). Comparative kinematic analysis and design optimization of redundant and nonredundant planar parallel manipulators intended for haptic use. *Robotica*, *38*, 1463-1477. https://doi.org/10.1017/S0263574719001577

[6] Liu, G., Wang, Y., Zhang, Y., & Xie, Z. (2015). Real-time solution of the forward kinematics for a parallel haptic device using a numerical approach based on neural networks, *Journal of Mechanical Science and Technology*, *29*, 2487-2499. https://doi.org/10.1007/s12206-015-0543-x

[7] Liu, S., Qiu, Z.-C., & Zhang, X.-M. (2017). Singularity and path-planning with the working mode conversion of a 3-

DOF 3-RRR planar parallel manipulator. *Mechanism and Machine Theory*, *107*, 166-182. https://doi.org/10.1016/j.mechmachtheory.2016.09.004

[8] Gao, Y., Chen, K., Gao, H., Xiao, P., & Wang, L. (2019). Small-angle perturbation method for moving platform orientation to avoid singularity of asymmetrical 3-RRR planner parallel manipulator. *Journal of the Brazilian Society of Mechanical Sciences and Engineering*, *41*. https://doi.org/10.1007/s40430-019-2012-4

[9] Gallant, A., Boudreau, R., & Gallant, M. (2012). Geometric determination of the dexterous workspace of n-RRRR and n-RRPR manipulators. *Mechanism and Machine Theory*, *51*, 159-171. https://doi.org/10.1016/j.mechmachtheory.2012.01.004

[10] Bihari, B., Kumar, D., Jha, C., Rathore, V. S., & Dash, A. K., (2016). A geometric approach for the workspace analysis of two symmetric planar parallel manipulators. *Robotica*, *34*, 738-763. https://doi.org/10.1017/S0263574714001830

[11] Ganesh, M., Bihari, B., Rathore, V. S., Kumar, D., Kumar, C., Sree, A. R., Sowmya, K. N., & Dash, A. K. (2017). Determination of the closed-form workspace area expression and dimensional optimization of planar parallel manipulators. *Robotica*, *35*, 2056-2075. https://doi.org/10.1017/S0263574716000710

[12] Dash, A. K., Chen, I.-M., Yeo, S. H., & Yang, G. L. (2005). Workspace generation and planning singularity-free path for parallel manipulators. *Mechanism and Machine Theory*, *40*, 776-805. https://doi.org/10.1016/j.mechmachtheory.2005.01.001

[13] Gosselin, C. & Angeles, J. (1988). The optimum kinematic design of a planar three-degree-of-freedom parallel manipulator. *Journal of Mechanisms, Transmissions, and Automation in Design*, *110*, 35-41. https://doi.org/10.1115/1.3258901

[14] Hosseini, M. A., Daniali, H.-R. M., & Taghirad, H. D. (2011). Dexterous workspace optimization of a tricept parallel manipulator. *Advanced Robotics*, *25*, 1697-1712. https://doi.org/10.1163/016918611X584640

[15] Engin, C. & Hellmuth, S. (2014). A planar parallel 3-RRR robot with synchronously driven cranks. *Mechanism and Machine Theory*, *79*, 29-45. https://doi.org/10.1016/j.mechmachtheory.2014.04.001

[16] Mohammadi Daniali, H. R., Zsombor-Murray, P. J., & Angeles, J. (1995). Singularity analysis of planar parallel manipulators. *Mechanism and Machine Theory*, *30*, 665-678.

[17] Bandyopadhyay, S. & Ghosal, A. (2004). Analysis of configuration space singularities of closed-loop mechanisms and parallel manipulators. *Mechanism and Machine Theory*, *39*, 519-544. https://doi.org/10.1016/j.mechmachtheory.2003.08.003

[18] Agarwal, A., Nasa, C., & Bandyopadhyay, S. (2016). Dynamic singularity avoidance for parallel manipulators using a task-priority based control scheme. *Mechanism and Machine Theory*, *96*, 107-126. https://doi.org/10.1016/j.mechmachtheory.2015.07.013

[19] Choi, J.-H., Seo, T., & Lee, J. W. (2013). Singularity analysis of a planar parallel mechanism with revolute joints based on a geometric approach. *International Journal of Precision Engineering and Manufacturing*, *14*, 1369-1375. https://doi.org/10.1007/s12541-013-0185-9

[20] Baron, N., Philippides, A., & Rojas, N. (2019). A novel kinematically redundant planar parallel robot manipulator with full rotatability. *Journal of Mechanisms and Robotics*, *11*. https://doi.org/10.1115/1.4041698

[21] Cha, S. H., Lasky, T. A., & Velinsky, S. A. (2007). Kinematically-redundant variations of the 3-RRR mechanism and local optimization-based singularity avoidance. *Mechanics Based Design of Structures and Machines*, *35*, 15-38. https://doi.org/10.1080/15397730601155626

[22] Cha, S.-H., Lasky, T. A., & Velinsky, S. A. (2009). Determination of the kinematically redundant active prismatic joint variable ranges of a planar parallel mechanism for singularity-free trajectories. *Mechanism and Machine Theory*, *44*, 1032-1044. https://doi.org/10.1016/j.mechmachtheory.2008.05.010

[23] Kucuk, S. (2013). Energy minimization for 3-RRR fully planar parallel manipulator using particle swarm optimization. *Mechanism and Machine Theory*, *62*, 129-149. https://doi.org/10.1016/j.mechmachtheory.2012.11.010

[24] Gao, Y., Chen, K., Gao, H., Zheng, H. M., Wang, L., & Xiao, P. (2020). Energy consumption prediction for 3-RRR PPM through combining LSTM neural network with Whale optimization algorithm. *Mathematical Problems in Engineering*, *2020*. https://doi.org/10.1155/2020/6590397

[25] Gosselin, C. & Angeles, J. (1990). Singularity analysis of closed-loop kinematic chains. *IEEE Transactions on Robotics and Automation*, *6*, 281-290. https://doi.org/10.1109/70.56660

[26] Leon, Steven J. (2006). *Linear Algebra with Applications*. Prentice Hall, New York, America.

Appendix A: The Sufficient Condition of the First Type of Singularity for the 3-RRR PPM and its Proof

In any branch chain of the 3-RRR PPM, if the active rod A_iB_i and passive rod B_iC_i are straightened or overlapped on the same straightline, then $\det(\boldsymbol{\Phi}_2) = 0$; that is, there must be the first singular phenomenon [15-17].

Proof of originality based on linear algebra [26] is given as follows.

Proof. As shown in Fig. 1, if A_1B_1 and B_1C_1 are straightened on the same straight line, then $\theta_1 = \theta_4$; if A_1B_1 and B_1C_1overlap on the same straight line, then $\theta_4 = \pi + \theta_1$. If A_2B_2 and B_2C_2 are straightened on the same straight line, then $\theta_2 = \theta_5$; if A_2B_2 and B_2C_2 overlap on the same straight line, then $\theta_2 = \pi + \theta_5$. If A_3B_3 and B_3C_3 are straightened on the same straight line, then $\theta_3 = \theta_6$; if A_3B_3 and B_3C_3 overlap on the same straight line, then $\theta_3 = \pi + \theta_6$.

Therefore, for the i^{th} (i = 1, 2, 3) branch chain of the 3-RRR PPM, if the active rod A_iB_i and passive rod B_iC_i are straightened on the same straightline, then:

$$\begin{cases} \sin\theta_i = \sin\theta_{i+3} \\ \cos\theta_i = \cos\theta_{i+3} \end{cases}, \tag{21}$$

If active rod A_iB_i and passive rod B_iC_i overlap on the same straightline, then:

$$\begin{cases} \sin\theta_i = -\sin\theta_{i+3} \\ \cos\theta_i = -\cos\theta_{i+3} \end{cases} \tag{22}$$

As shown in Fig. 1, when the active rod A_iB_i and passive rod B_iC_i of any branch chain are straightened on the same straightline and the vector $\boldsymbol{B_iC_i}$ is projected onto the x-and y-axes, combined with Eq. (16), the following condition can be obtained:

$$\begin{cases} l_{i+3}\cos\theta_{i+3} = l_{i+3}\cos\theta_i = x_{Ci} - x_{Bi} \\ l_{i+3}\sin\theta_{i+3} = l_{i+3}\sin\theta_i = y_{Ci} - y_{Bi} \end{cases} \tag{23}$$

Combining Eqs. (2), (5), (6), and (23), the three non-zero elements of the diagonal matrix $\boldsymbol{\Phi}_2$ in Eq. (13) are further reduced as follows:

$$\begin{aligned}&l_i\left(M_i\sin\theta_i-N_i\cos\theta_i\right)\\&=l_i[\left(x_{Ci}-x_{Ai}\right)\sin\theta_i-\left(y_{Ci}-y_{Ai}\right)\cos\theta_i\\&=l_i[(l_{i+3}\cos\theta_i+x_{Bi}-x_{Ai})\sin\theta_i-\\&-\left(l_{i+3}\sin\theta_i+y_{Bi}-y_{Ai}\right)\cos\theta_i]=\\&=l_i[(l_{i+3}\cos\theta_i+l_i\cos\theta_i)\sin\theta_i-\\&-\left(l_{i+3}\sin\theta_i+l_i\sin\theta_i\right)\cos\theta_i]=0\end{aligned}\tag{24}$$

From Eqs. (13) and (24), it can be deduced that when the active rod A_iB_i and passive rod B_iC_i of any branch chain of the 3-RRR PPM are straightened on the same straightline, det($\boldsymbol{\Phi}_2$) = 0. Similarly, when the active rod A_iB_i and passive rod B_iC_i of any branch chain overlap on the same straightline and the vector $\boldsymbol{B_iC_i}$ is projected onto the x- and y-axes, combined with Eq. (17), following the above steps presents following condition:

$$\begin{cases}l_{i+3}\cos\theta_{i+3}=-l_{i+3}\cos\theta_i=x_{Ci}-x_{Bi}\\l_{i+3}\sin\theta_{i+3}=-l_{i+3}\sin\theta_i=y_{Ci}-y_{Bi}\end{cases}\tag{25}$$

Similarly, it can be deduced that if the active rod A_iB_i and passive rod B_iC_i of any branch chain of the 3-RRR PPM overlap on the same straightline, then det($\boldsymbol{\Phi}_2$) = 0.

Appendix B: The Necessary and Sufficient Condition of the Second Type of Singularity for the 3-RRR PPM and Their Proofs

The second type of singularity occurs for the 3-RRR PPM if and only if the three different straight lines that belong to the passive rods B_1C_1, B_2C_2, and B_3C_3 are concurrent or parallel, or any two of the three straight lines B_1C_1, B_2C_2, and B_3C_3 are parallel and collinear [8, 15-17].

Proof of originality based on linear algebra [26] is given as follows.

Proof. To distinguish the centroid coordinate (x, y) of the moving platform, the coordinate of the moving point on the straight line B_iC_i is marked as (u, v), and the equation of the straight line B_iC_i is represented as:

$$\left(y_{Ci}-y_{Bi}\right)u+\left(-x_{Ci}+x_{Bi}\right)v+y_{Bi}x_{Ci}-y_{Ci}x_{Bi}=0\tag{26}$$

The augmented matrix of Eq. (26) is denoted by $\boldsymbol{\Phi}_C$, and its determinant is.

$$\det(\boldsymbol{\Phi}_C)=\begin{vmatrix}y_{C1}-y_{B1} & x_{B1}-x_{C1} & y_{B1}x_{C1}-y_{C1}x_{B1}\\y_{C2}-y_{B2} & x_{B2}-x_{C2} & y_{B2}x_{C2}-y_{C2}x_{B2}\\y_{C3}-y_{B3} & x_{B3}-x_{C3} & y_{B3}x_{C3}-y_{C3}x_{B3}\end{vmatrix}\tag{27}$$

The first and second columns of Eq. (27) are rearranged as follows to establish the relationship between det($\boldsymbol{\Phi}_C$) and the determinant det($\boldsymbol{\Phi}_y$) of the discriminant matrix of the second type of singularity.

From Eqs. (1), (2), (4), and (5), Eqs. (28) and (29) can be obtained as:

$$\begin{aligned}&y_{Ci}-y_{Bi}=y+x_{Ci}'\sin\theta+y_{Ci}'\cos\theta-\\&-\left(y_{Ai}+l_i\sin\theta_i\right)=-\left(l_i\sin\theta_i-N_i\right)\end{aligned}\tag{28}$$

$$\begin{aligned}&x_{Bi}-x_{Ci}=-\left(x+x_{Ci}'\cos\theta-y_{Ci}'\sin\theta\right)+x_{Ai}+\\&+l_i\cos\theta_i=l_i\cos\theta_i-M_i\end{aligned}\tag{29}$$

Therefore, the sum of the first column of det($\boldsymbol{\Phi}_C$) and second column of det($\boldsymbol{\Phi}_y$) is zero, and the first column of det($\boldsymbol{\Phi}_y$) and second column of det($\boldsymbol{\Phi}_C$) are equal. The third column of det($\boldsymbol{\Phi}_C$) is marked as:

$$C_{Ci}=y_{Bi}x_{Ci}-y_{Ci}x_{Bi}\tag{30}$$

Based on Eqs. (2), (4), and (5), the third column of Eq. (14) is simplified as follows:

$$\begin{aligned}&(l_i\sin\theta_i-N_i)\left(M_i+x_{Ai}-x\right)-\\&-\left(l_i\cos\theta_i-M_i\right)\left(N_i+y_{Ai}-y\right)\\&=\left(y_{Bi}-y_{Ci}\right)\left(x_{Ci}-x\right)-\left(x_{Bi}-x_{Ci}\right)\left(y_{Ci}-y\right)\\&=y_{Bi}x_{Ci}-y_{Ci}x_{Bi}+x\left(y_{Ci}-y_{Bi}\right)-y\left(x_{Ci}-x_{Bi}\right)\\&=C_{Ci}+x\left(y_{Ci}-y_{Bi}\right)-y\left(x_{Ci}-x_{Bi}\right)\end{aligned}\tag{31}$$

Based on the conditions: $xy \neq 0$ and $xy = 0$, four cases can be established. The relationship between det($\boldsymbol{\Phi}_C$) and det($\boldsymbol{\Phi}_y$) is discussed as follows:

(1) When $x \neq 0$ and $y \neq 0$, according to Eqs. (14) and (27) to (31), combining the properties of the determinant det($\boldsymbol{\Phi}_y$) multiplied by xy, Eq. (32) can be obtained:

$$\begin{aligned}xy\det(\boldsymbol{\Phi}_y)&=\begin{vmatrix}y(x_{C1}-x_{B1}) & -x(y_{C1}-y_{B1}) & C_{C1}+x\left(y_{C1}-y_{B1}\right)-y\left(x_{C1}-x_{B1}\right)\\y(x_{C2}-x_{B2}) & -x(y_{C2}-y_{B2}) & C_{C2}+x\left(y_{C2}-y_{B2}\right)-y\left(x_{C2}-x_{B2}\right)\\y(x_{C3}-x_{B3}) & -x(y_{C3}-y_{B3}) & C_{C3}+x\left(y_{C3}-y_{B3}\right)-y\left(x_{C3}-x_{B3}\right)\end{vmatrix}\\&=-\begin{vmatrix}y(x_{C1}-x_{B1}) & -x(y_{C1}-y_{B1}) & C_{C1}\\y(x_{C2}-x_{B2}) & -x(y_{C2}-y_{B2}) & C_{C2}\\y(x_{C3}-x_{B3}) & -x(y_{C3}-y_{B3}) & C_{C3}\end{vmatrix}=xy\begin{vmatrix}y_{C1}-y_{B1} & x_{B1}-x_{C1} & C_{C1}\\y_{C2}-y_{B2} & x_{B2}-x_{C2} & C_{C2}\\y_{C3}-y_{B3} & x_{B3}-x_{C3} & C_{C3}\end{vmatrix}=xy\det\left(\boldsymbol{\Phi}_C\right)\end{aligned}\tag{32}$$

Hence, det($\boldsymbol{\Phi}_y$) = det($\boldsymbol{\Phi}_C$) can be obtained using Eq. (32).

(2) When $x = 0$ and $y \neq 0$, a similar condition is obtained:

$$\begin{aligned}&y\det(\boldsymbol{\Phi}_y)=\\&-\begin{vmatrix}y(x_{C1}-x_{B1}) & -(y_{C1}-y_{B1}) & C_{C1}-y\left(x_{C1}-x_{B1}\right)\\y(x_{C2}-x_{B2}) & -(y_{C2}-y_{B2}) & C_{C2}-y\left(x_{C2}-x_{B2}\right)\\y(x_{C3}-x_{B3}) & -(y_{C3}-y_{B3}) & C_{C3}-y\left(x_{C3}-x_{B3}\right)\end{vmatrix}\end{aligned}\tag{33}$$

$$= -\begin{vmatrix} y(x_{C1}-x_{B1}) & -(y_{C1}-y_{B1}) & C_{C1} \\ y(x_{C2}-x_{B2}) & -(y_{C2}-y_{B2}) & C_{C2} \\ y(x_{C3}-x_{B3}) & -(y_{C3}-y_{B3}) & C_{C3} \end{vmatrix} = y\det(\boldsymbol{\Phi}_C)$$

Therefore, $\det(\boldsymbol{\Phi}_y) = \det(\boldsymbol{\Phi}_C)$ can be obtained using Eq. (33).

(3) When $x \neq 0$ and $y = 0$, the following condition is obtained:

$$x\det(\boldsymbol{\Phi}_y) = x\det(\boldsymbol{\Phi}_C) \tag{34}$$

Therefore, $\det(\boldsymbol{\Phi}_y) = \det(\boldsymbol{\Phi}_C)$ can be obtained using Eq. (34).

(4) When $x = 0$ and $y = 0$, according to Eqs. (14) and (27) to (31), the following is obtained:

$$\det(\boldsymbol{\Phi}_y) = \det(\boldsymbol{\Phi}_C) \tag{35}$$

Therefore, $\det(\boldsymbol{\Phi}_y) = \det(\boldsymbol{\Phi}_C)$ is always true.

According to the five possible cases, which are the possible geometric relationships among the three straight lines B_1C_1, B_2C_2, and B_3C_3 on the same plane, the values of $\det(\boldsymbol{\Phi}_C)$ are discussed as follows:

Case 1: The three different straight lines B_1C_1, B_2C_2, and B_3C_3 are concurrent if and only if $\det(\boldsymbol{\Phi}_C) = 0$ [26].

Case 2: If the three different straight lines B_1C_1, B_2C_2, and B_3C_3 are parallel to each other, then $\det(\boldsymbol{\Phi}_C) = 0$.

According to Eq. (26), under these circumstances, y_{Ci}-$y_{Bi} = k(x_{Ci} - x_{Bi})$ when the three straight lines are parallel to each other, and according to Eq. (27), the elements of the first column are proportional to those of the second column in Eq. (24); therefore, $\det(\boldsymbol{\Phi}_C) = 0$.

Case 3: If any two of the three straight lines B_1C_1, B_2C_2, and B_3C_3 are parallel and collinear, that is, any two of them are coincident on the same straight line, then $\det(\boldsymbol{\Phi}_C) = 0$.

According to Eq. (27), under these circumstances, the two rows of the three-row elements are proportional to each other in Eq. (24), and it can be inferred that $\det(\boldsymbol{\Phi}_C) = 0$.

Case 4: If any two of the three straight lines B_1C_1, B_2C_2, and B_3C_3 are parallel but not coincident on the same straight line and the third straight line intersects with them, then $\det(\boldsymbol{\Phi}_C) \neq 0$.

Without losing generality, if $B_1C_1$is parallel to B_2C_2 and B_3C_3 is not parallel to B_1C_1 and B_2C_2, the equations of the straight lines B_iC_i can be assumed to be $v = k_1u + b_1$, $v = k_2u + b_2$, and $v = k_3u + b_3$ (where $k_1 = k_2$, $b_1 \neq b_2$, and $k_1 = k_2 \neq k_3$), and $\det(\boldsymbol{\Phi}_C)$ is expanded as follows in accordance with the algebraic complement of the third column in Eq. (27):

$$\det(\boldsymbol{\Phi}_C) = \begin{vmatrix} k_1 & -1 & b_1 \\ k_2 & -1 & b_2 \\ k_3 & -1 & b_3 \end{vmatrix} = (k_1 - k_3)(b_1 - b_2) \neq 0 \tag{36}$$

Case 5: If the three different straight lines B_1C_1, B_2C_2, and B_3C_3 are not concurrent and any two straight lines intersect at different points, then $\det(\boldsymbol{\Phi}_C) \neq 0$.

According to **Case 1**, $\det(\boldsymbol{\Phi}_C) \neq 0$ can be proved by the reduction to absurdity.

Therefore, if $\det(\boldsymbol{\Phi}_C) = 0$, one of the following relationships must be satisfied among the three straight lines B_1C_1, B_2C_2, and B_3C_3:(1) the three different straight lines B_1C_1, B_2C_2, and B_3C_3 are concurrent; (2) the three different straight lines B_1C_1, B_2C_2, and B_3C_3 are parallel to each other; and (3) any two of the three different straight lines B_1C_1, B_2C_2, and B_3C_3 are parallel and collinear and vice versa.

Contact information:

Yin GAO, Lecturer
(Corresponding author)
School of mechanical engineering,
Hefei University of Technology,
Hefei, Anhui, 230009, P. R. China
E-mail: gy0203@mail.hfut.edu.cn

Ke CHEN, PhD, Full Professor
School of mechanical engineering,
Hefei University of Technology,
Hefei, Anhui, 230009, P. R. China
E-mail: k.chen@163.com

Hong GAO, PhD, Full Professor
School of mechanical engineering,
Anhui Polytechnic University,
241000 Wuhu, Anhui, 241000, P. R. China
E-mail: gaohong0706@sina.com

Hongmei ZHENG, PhD, Full Professor
School of mechanical engineering,
Hefei University of Technology,
Hefei, Anhui, 230009, P. R. China
E-mail: Hongmeizh@hfut.edu.cn

Lulu WU, PhD, Vice Professor
School of mechanical engineering,
Anhui Polytechnic University,
241000 Wuhu, Anhui, 241000, P. R. China
E-mail: wull@ahpu.edu.cn

Ping XIAO, PhD, Full Professor
School of mechanical engineering,
Anhui Polytechnic University,
241000 Wuhu, Anhui, 241000, P. R. China
E-mail: tlxp95@163.com